BOLLETTINO DI GEOFISICA TEORICA ED APPLICATA VOL. XXXIV, N. 134-135 - JUNE-SEPTEMBER 1992

P. COSENTINO, E. GAGLIANO CANDELA, D. LUZIO

INTEGRATED GEOELECTRICAL INVESTIGATIONS ON THE EAST HILL IN THE SELINUNTE ARCHAEOLOGICAL PARK

Abstract. A geoelectrical study was carried out in the Selinunte area within the framework of a geophysical survey intended to test the feasibility of an archaeological program. This pilot program involves several Italian research groups. The survey was conceived to obtain high detail and reliability in the results for a small area in which previous geomagnetic investigations have shown some anomalies. In that area, measuring 11 m×11 m, a square grid of 144 copper electrodes was used to obtain 1548 apparent resistivity measurements, using the tripotential method, dipole-dipole profiling, and rectangle configurations. The results were used to construct a set of maps and pseudo-sections. The various sets of data were compared and also used in a variety of different combinations to test both their resolving power and reliability. On the whole, it seems that this kind of geophysical approach could give appreciable results in surveying archaeological sites. In fact, an only slightly greater effort in field operations significantly increases the amount of experimental data, giving much more reliable information, which can be interpreted using integrated inversion methods.

Nevertheless, without any specific target to the research, it is difficult to relate the anomalies detected in the area with geological or archaeological sources.

INTRODUCTION

The investigated area is located on the eastern hill of the archaeological park of Selinunte (south-western Sicily, see Fig. 1), about 300 m north of Apollo's Temple (temple G), just where a Roman settlement has been tentatively identified (Fig. 2).

This area is a small section (11 m×11 m) of the so-called "40×40" square area (Fig. 3), which was selected for detailed integrated geophysical surveys. Previously in that small area, a sharp magnetic anomaly was detected using both a Geoscan FM 36 Fluxgate magnetometer (Piro et al., 1991) and an MP3 gradiometer (Bozzo and Merlanti, 1991). This anomaly, however, was not evident in the georadar survey by Piro et al. (1991).

The average electro-stratigraphic settlement down to about ten meters was investigated by Lapenna et al. (1991) and by Amadori and Versino (1991). The V.E.S located near the 40×40 area have shown the presence of a thin layer (0.8-1.0 m) of soil with resistivity 20-80 Ohm.m. This layer overlies 2-3 m of calcarenites, with resistivity ranging from 120 to 170 Ohm.m, followed by 6-10 m of sandy clays of low resistivity values (10-15 Ohm.m). These clays lie on a different clay substratum (with typical resistivity of the order of 3-4 Ohm.m).

In summary, from the whole data set, it is apparent that the calcarenite layer is not everywhere recognizable.

THE EXPERIMENTAL SURVEY

The 11 m×11 m area was covered by a square grid of copper electrodes using a square

Manuscript received February 26, 1992; accepted March 18, 1992.

Istituto di Geofisica Mineraria, University, via M. Stabile 110, Palermo, Italy.

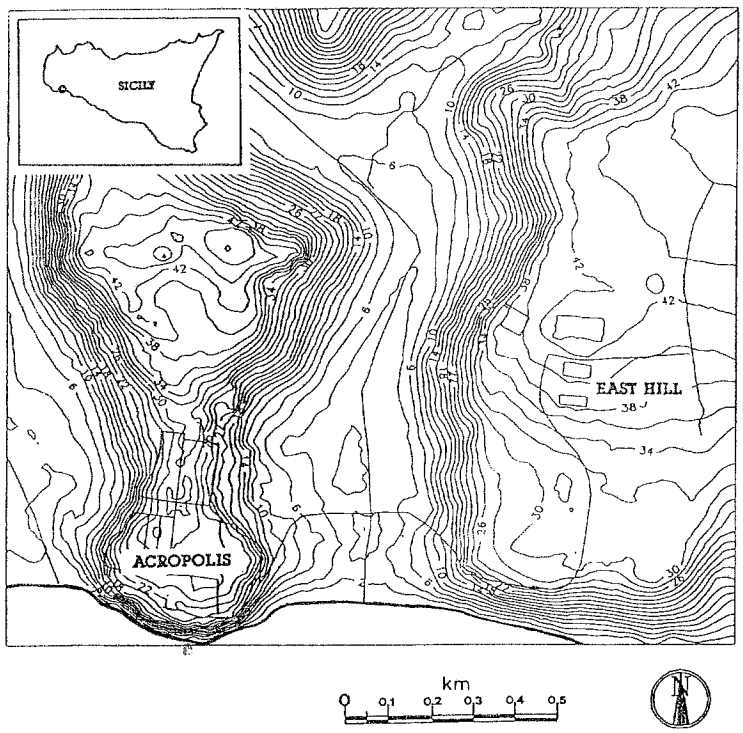

Fig. 1 — Map of the national archeological park of Selinunte.

mesh of 1 m side. The 144 electrodes were used in turn both as trasmitter and receiver probes. The apparent resistivity values were calculated starting from the current and potential measurements, which were taken in both the N-S and the E-W directions, using the following arrays:

- Wenner (W), axial-dipole (AD) and crossing-dipole (CD) arrays: a totale of 324 measurements in each direction, to perform a "Tripotential" survey (Carpenter and Habberjam, 1956; Habberjam, 1979).

- dipole-dipole axial arrays, the order n (which indicates the center-distance as integer multiple of AB=MN) ranging from 2 to 5. On the whole, 360 measurements were taken, in each direction, in order to reconstruct two-dimensional pseudo-sections.

- rectangle arrays using AB=120 m and 60 m: a total of 288 measurements in the N-S direction. The same, but using AB=50 m, with 144 measurements, was carried out in the E-W direction.

The experimental current and potential data were collected using an apparatus having sensibilities of 0.1 mA and 0.1 mV. Some measurements at random were repeated in order to evaluate their reliability as well as the relative probable errors. The mean probable relative error on the apparent resistivity estimates, as evaluated on the basis of the experimental results, is less than 0.75% for the tripotential measurements, less than 2.5% for high order dipole-dipole arrays, but quickly decreases for the lower order ones. The probable relative errors for the rectangle array measurements were as large as 10-15%. These errors were partially removed using suitable filtering techniques.

DATA PROCESSING

The apparent resistivity data were collected and suitably processed in order to obtain different

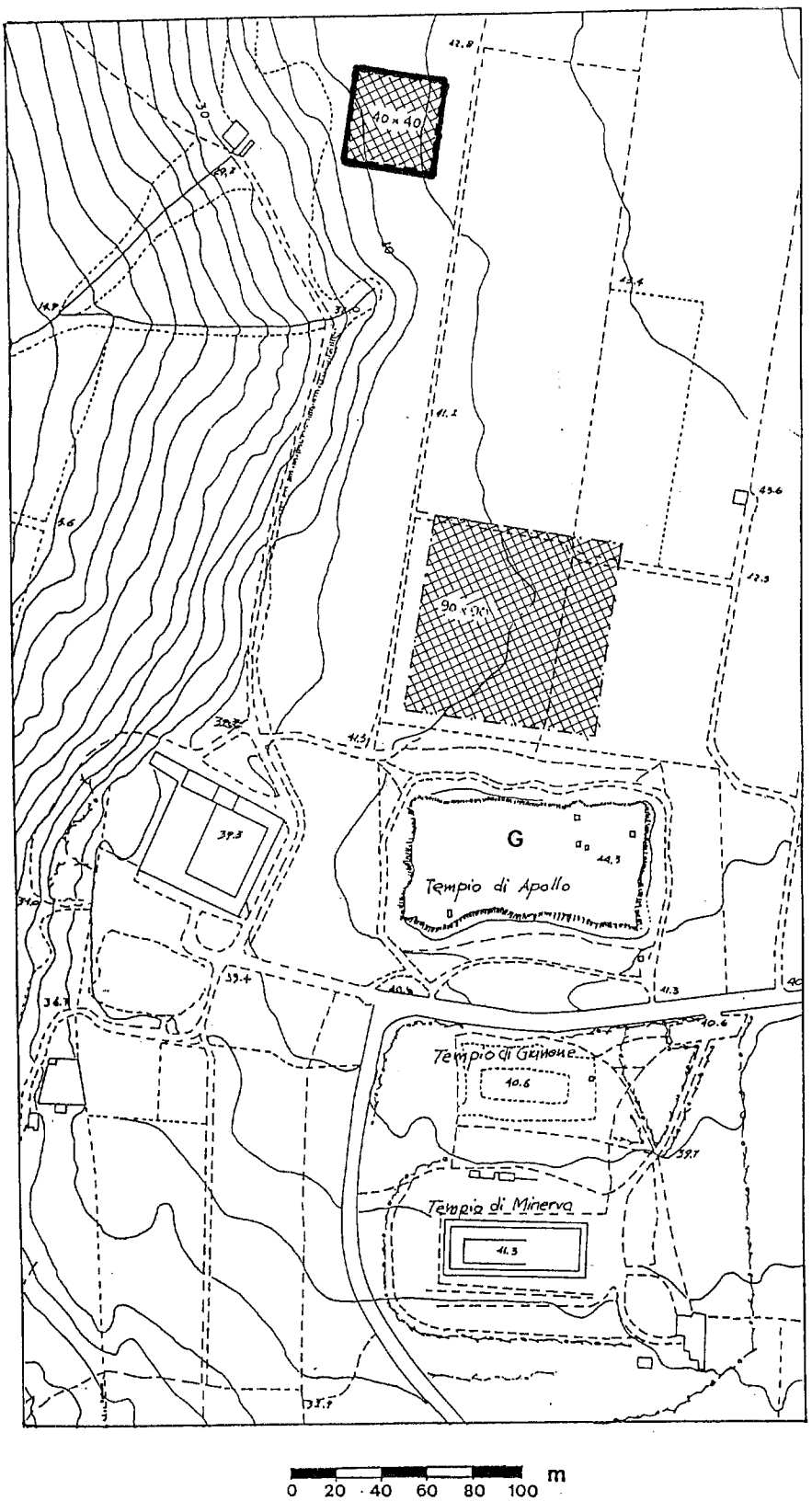

Fig. 2 — The location of the 40×40 area on the Eastern Hill.

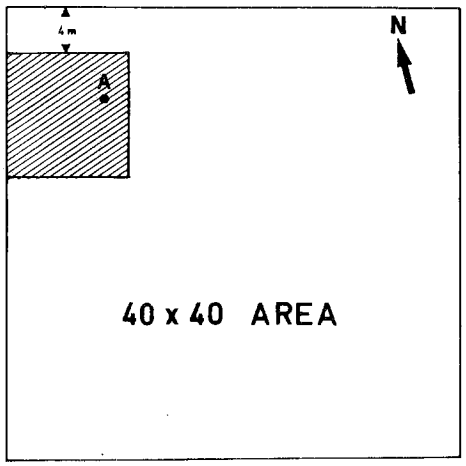

Fig. 3 — Location of the investigated area (dashed) and the magnetic anomaly (A) in the "40×40" area.

pictures of the resistivity space distribution.

Depending on the arrays and methodologies used, the processing of the various data sets was carried out in different ways, but the general characteristics of the processing techniques include the following steps:

- correction of the data (Tripotential method only).
- association of the corrected apparent resistivity values with representative points of the investigated volumes.
- comparison and integration of the data measured using N-S and E-W oriented arrays.
- interpolation of the data over a set of regular grid points for processing, graphic representation and comparison.
- two-dimensional filtering of the data.
- separation of the "apparent resistivity field" into component fields which can be related to simple-shaped anomalies.

Tripotential measurements

In this method, the hypothetical - error free - experimental data, for theoretical reasons which are independent of the resistivity space distribution, are interconnected by the following relationship:

$$Rw - Rcd - Rad = 0, \tag{1}$$

where *Rw*, *Rcd* and *Rad* are the three "resistances" measured respectively with the Wenner, crossing-dipole and axial-dipole arrays using the same four electrodes. Thus, when an equispaced array is used, the following relation between the corresponding apparent resistivities arises:

$$3\,\varrho w - 2\,\varrho cd - \varrho ad = 0. \tag{2}$$

Due to experimental errors, eqns. (1) and (2) become

$$Rw - Rcd - Rad = e, \tag{3}$$

$$3\,\varrho w - 2\,\varrho cd - \varrho ad = Kad\ e = E, \tag{4}$$

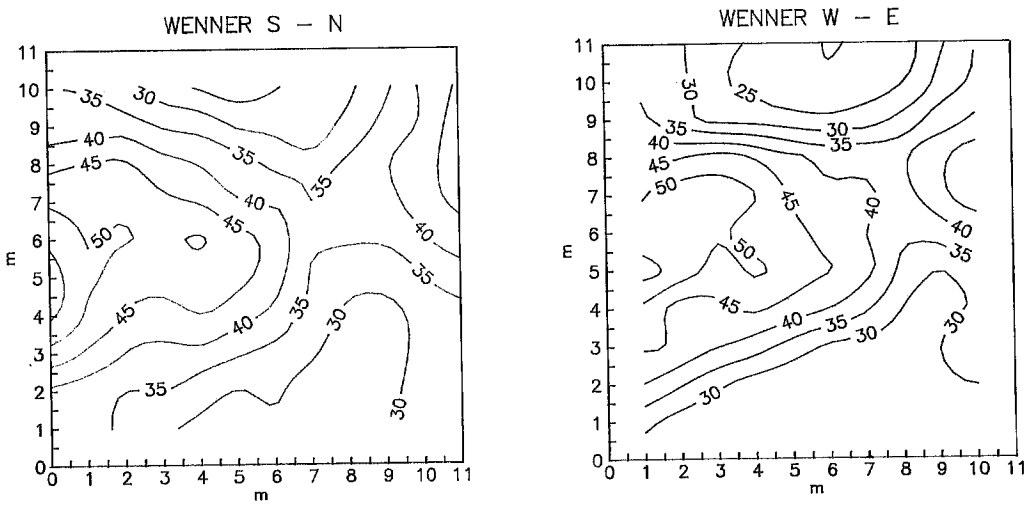

Fig. 4 — The two maps obtained using Wenner arrays in S-N (left) and W-E (right) directions.

where e and E are the inclusive errors in the three resistences and apparent resistivities, respectively, $Kad=6.\pi.p$ is the geometric factor of the axial-dipole array, and p is the electrode spacing.

The constraint due to eqn. (2) implies that in the three-resistivities space, a correct measurement is a point on the plane which crosses the origin (0, 0, 0) having direction numbers 3 (on the ϱw axis), —2 (on the ϱcd axis) and —1 (on the ϱad axis). A point representing an experimental measurement characterized by an error E will belong to a plane which is parallel to the previous one but at a distance of $E\cdot\sqrt{14}/14$.

The correction of the errors on the i-th tripotential measurements should be accomplished, in principle, using a suitable vector connecting the experimental point to the $E=0$ plane. The choice of the correction vectors could be submitted to a probability criterion, e.g., using the variances of the various resistivity values. In this case, an elliptic target area can be traced in the $E=0$ plane using the "virtual" confidence ellipsoid calculated at the selected confidence value and centered in the measurement point. This ellipsoid is virtual because it is calculated without the constraint given by eqn. (2).

Generally, it can be assumed that the probable errors are quite constant in the whole set of data, so that the virtual ellipsoid becomes a sphere and the elliptic confidence target area becomes a circle with center at the point ($\varrho w—3E/14$, $\varrho cd+E/7$, $\varrho ad+E/14$), which is the orthogonal projection of the experimental point onto the plane $E=0$. The radius of this confidence area is $\sqrt{(K^2\ \sigma^2—E^2/14)}$, where K is a coefficient connected with the selected confidence level and σ^2 is the measurement variance.

Different strategies for performing the corrections are possible. The simplest is to translate the experimental points directly onto the plane $E=0$ using a vector perpendicular to the target plane. The data can be so corrected using the expressions for the coordinates of the center of the above confidence circle. Another strategy is to assume that the errors are proportional to the measured values, as proposed by Habberjam (1979); the resulting corrections are the following:

$$\varrho w_c=\varrho w—E\ \varrho w/(3\varrho w+2\varrho cd+\varrho ad), \tag{5}$$

$$\varrho cd_c=\varrho cd+E\ \varrho cd/(3\varrho w+2\varrho cd+\varrho ad), \tag{6}$$

$$\varrho ad_c=\varrho ad+E\ \varrho ad/(3\varrho w+2\varrho cd+\varrho ad). \tag{7}$$

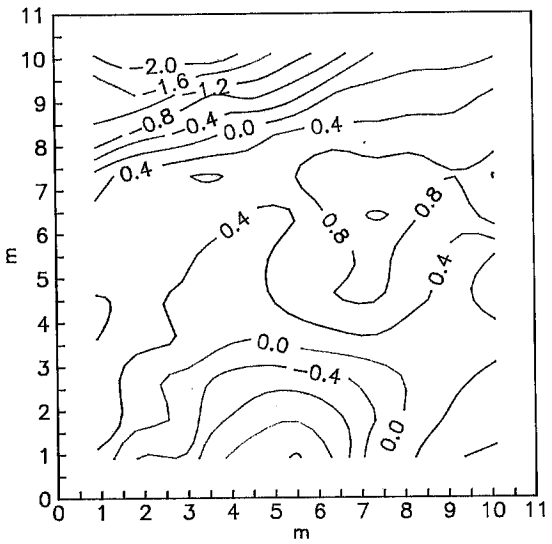

Fig. 5 — Map of the space distribution of the azimuthal heterogeneities index for Wenner apparent resistivities, calculated from 2 (ϱ[S-N]—ϱ[W-E])/(ϱ[S-N)]+ϱ[W-E]).

Other correction strategies impose some constraints upon the experimental data, coming from general assumptions on the anomaly source: this could imply a particular correlation low among the data in the resistivity space.

It is obvious that on an homogeneous earth the three resistivity values should be equal. So that in a quasi-homogeneous earth this condition can be imposed, leading to

$$\varrho w_c = \varrho w + (-2\varrho w + \varrho cd + \varrho ad)/3, \tag{8}$$

$$\varrho cd_c = \varrho cd + (\varrho w - 2\varrho cd + \varrho ad)/3, \tag{9}$$

$$\varrho ad_c = \varrho ad + (\varrho w + \varrho cd - 2\varrho ad)/3. \tag{10}$$

This correction, which is equivalent to calculating the arithmetic average of the three resistivities, can produce strong corrections of the experimental data, often much larger than

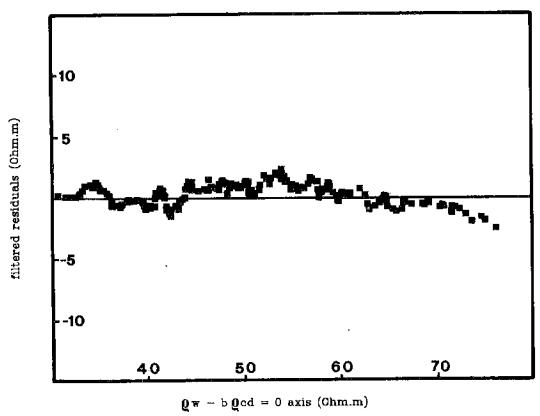

Fig. 6 — Low-pass filtered behaviour of the *b*-residuals in the resistivity domain.

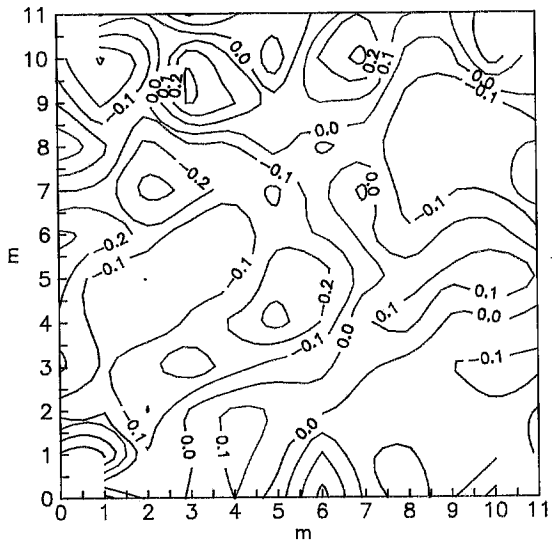

Fig. 7 — Map of the space distribution of the *b*-residuals.

the probable errors in the measurements. Actually, different values of the three resistivities may result from lateral and/or vertical unexposed variations in resistivity. However, this kind of correction can be used to evaluate some heterogeneity indices starting from the statistical distribution of the correction values.

Different general models can be selected which impose other linear or nonlinear correlations between the different resistivities values. The simplest relation is represented by the following equations:

$$\varrho w = b\ \varrho cd, \tag{11}$$

$$\varrho w = c\ \varrho ad = b\ \varrho ad/(3b-2), \tag{12}$$

$$\varrho cd = d\ \varrho ad = \varrho ad/(3b-2). \tag{13}$$

Eqns. (12) and (13) are easily obtained from eqns. (11) and (2).

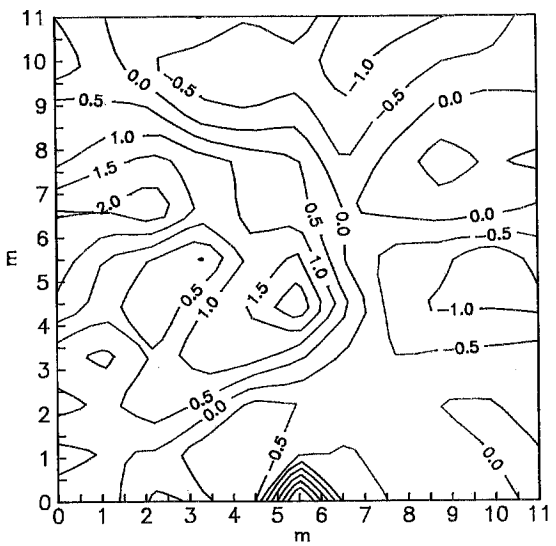

Fig. 8 — Low-pass filtered space distribution of the *b*-residuals.

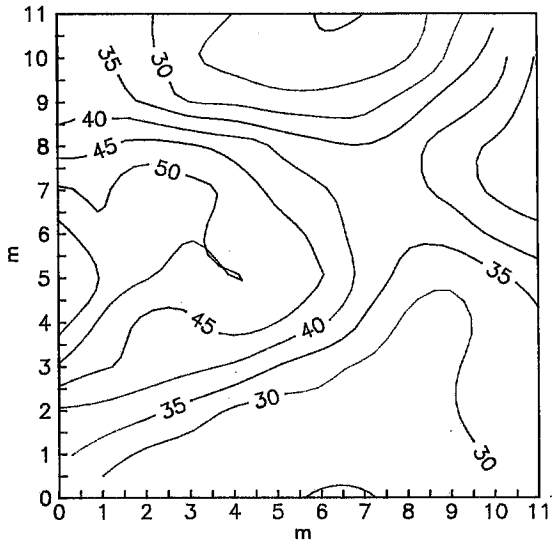

Fig. 9 — Map of the space distribution of the average resistivity-values of the three tripotential measures in all the points (both in N-S and W-E directions).

A least-squares estimate of the parameter b can be done using all the experimental data in the three-dimensional space of apparent resistivities, considering as error function the sum of the squared values of the distances between the experimental points and the straight line lying on the $E=0$ plane:

$$\varrho w/b=\varrho cd=\varrho ad/(3b-2). \tag{14}$$

This estimate of b can be used to calculate the corrections which are compatible with eqns. (2) and (14).

Thus, the corrected values are calculated as

$$\varrho w_c=\varrho w+(-(9b^2-12b+5)\ \varrho w+b\varrho cd+(3b^2-2b)\ \varrho ad)/D, \tag{15}$$

$$\varrho cd_c=\varrho cd+(b\varrho w-(10b^2-12b+4)\ \varrho cd+(3b-2)\ \varrho ad)/D, \tag{16}$$

$$\varrho ad_c=\varrho ad+((3b^2-2b)\ \varrho w+(3b-2)\ \varrho cd-(b^2+1)\ \varrho ad)/D, \tag{17}$$

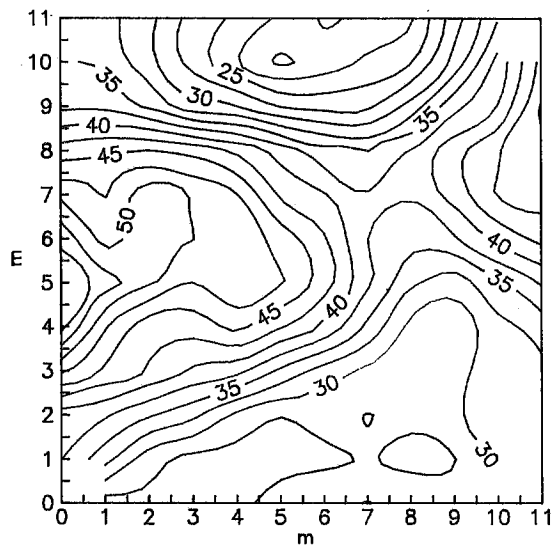

Fig. 10 — Low-pass filtered map of the average values of the N-S and W-E three tripotential resistivity data (Fig. 9).

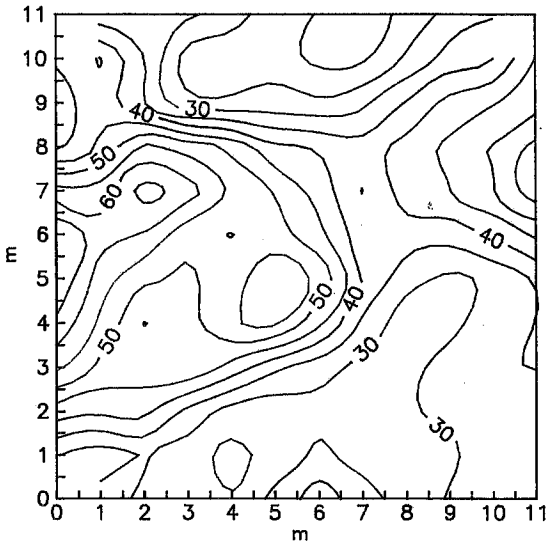

Fig. 11 — Low-pass filtered map of the W-E and N-S Wenner apparent resistivities.

where $D=10b^2-12b+5$.

Eqns. (15), (16) and (17) reduce, respectively, to eqns. (8), (9) and (10) when $b=1$.

Some general caracteristics of the buried heterogeneities can be deduced from the estimate of b and the connected standard deviation, as well as from a study of the correlation laws for the residuals both in the space and resistivity domains (Cosentino and Luzio, 1992).

An homogeneous earth should be characterized by $b=1$, by a standard deviation value comparable with the probable measurements error, and by no correlations between the residuals in both domains.

An earth containing randomly distributed heterogeneities should be characterized by a b-value close to one and by a large mean square value of the regression residuals: it grows depending on the average dimensions of the heterogeneities with respect to the dimensions of the investigated area and on the resistivity contrast.

When a one-dimensional layered model suitably represents the actual geological situation, depending on the spacing used and the thicknesses of the layers and their resistivity contrasts,

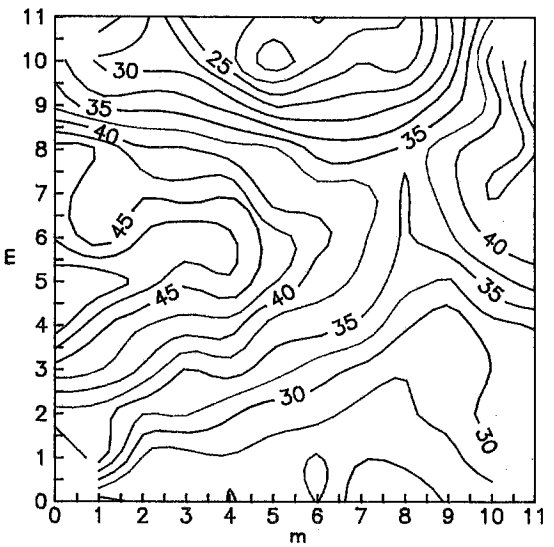

Fig. 12 — Low-pass filtered map of the N-S and W-E crossing dipole (*cd*) apparent resistivities.

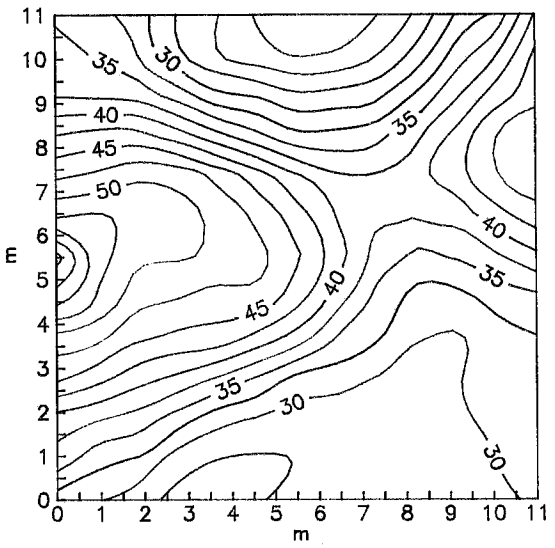

Fig. 13 — Low-pass filtered map of the N-S and W-E axial dipole (*ad*) apparent resistivities.

the value of *b* can be different from one (Cosentino and Luzio, 1992), but it is expected to have low and uncorrelated residuals.

Finally, the presence of recognizable and circumscribed heterogeneities is connected with the following characteristics:

- the *b* value can be significantly different from one,
- the residuals will be to some extent correlated both in the resistivity and space domains.

Dipole-dipole measurements

The processing of the dipole-dipole data was done in the classic way to obtain pseudo-sections along the investigated profiles.

Furthermore, Fraser's (1981) filter was applied along every profiles in the N-S and E-W directions, in order to have a planar view of the whole data set and to construct a contour map for the depth investigated.

Rectangle measurements

The data collected with the rectangle method generally have a low signal/noise ratio. So, even if the resulting maps are generally connected with deeper investigation than those previously examined, the experimental signal shows a larger relative amplitude of the high-frequency components. Thus, the data were processed in a simple way, mainly using appropriate low-pass filtering techniques to reduce the high-frequency noise.

COMPARISON AND INTEGRATION OF THE DATA

The tripotential data have very small experimental errors *Ei* expressed by eqn. (4), lower than 0.2%. Their spatial distribution seems to be random. All the collected data were corrected using eqns. (5), (6) and (7).

It is observed from the maps that the two sets of data acquired using the Wenner array (both E-W and S-N directions, Fig. 4), as well as those from the axial-dipole and crossing-dipole, seem to match each other very well. This means that no anisotropy, nor large lateral anomalies are recognizable. A quantitative check of this matching was performed using the azimuthal heterogeneity index and the resulting contour map is presented in Fig. 5.

The set of integrated (W-E and S-N) data for the three different arrays involved in the tripotential method seem very similar both in spatial trend and absolute values since eqns. (11)-(13)

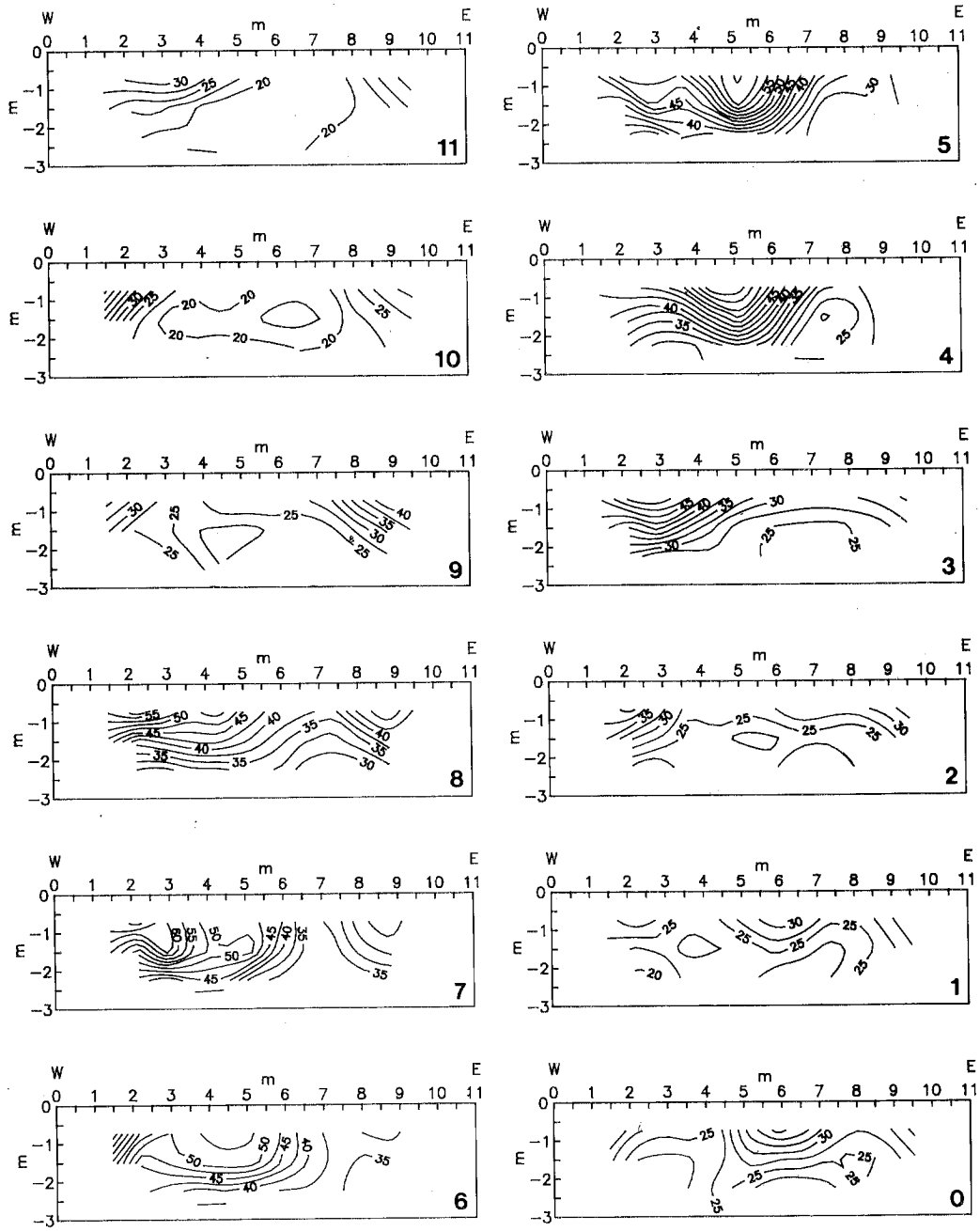

Fig. 14 — Set of pseudo-sections from axial dipole resistivity data (measured in W-E direction) from north (11) to south (0).

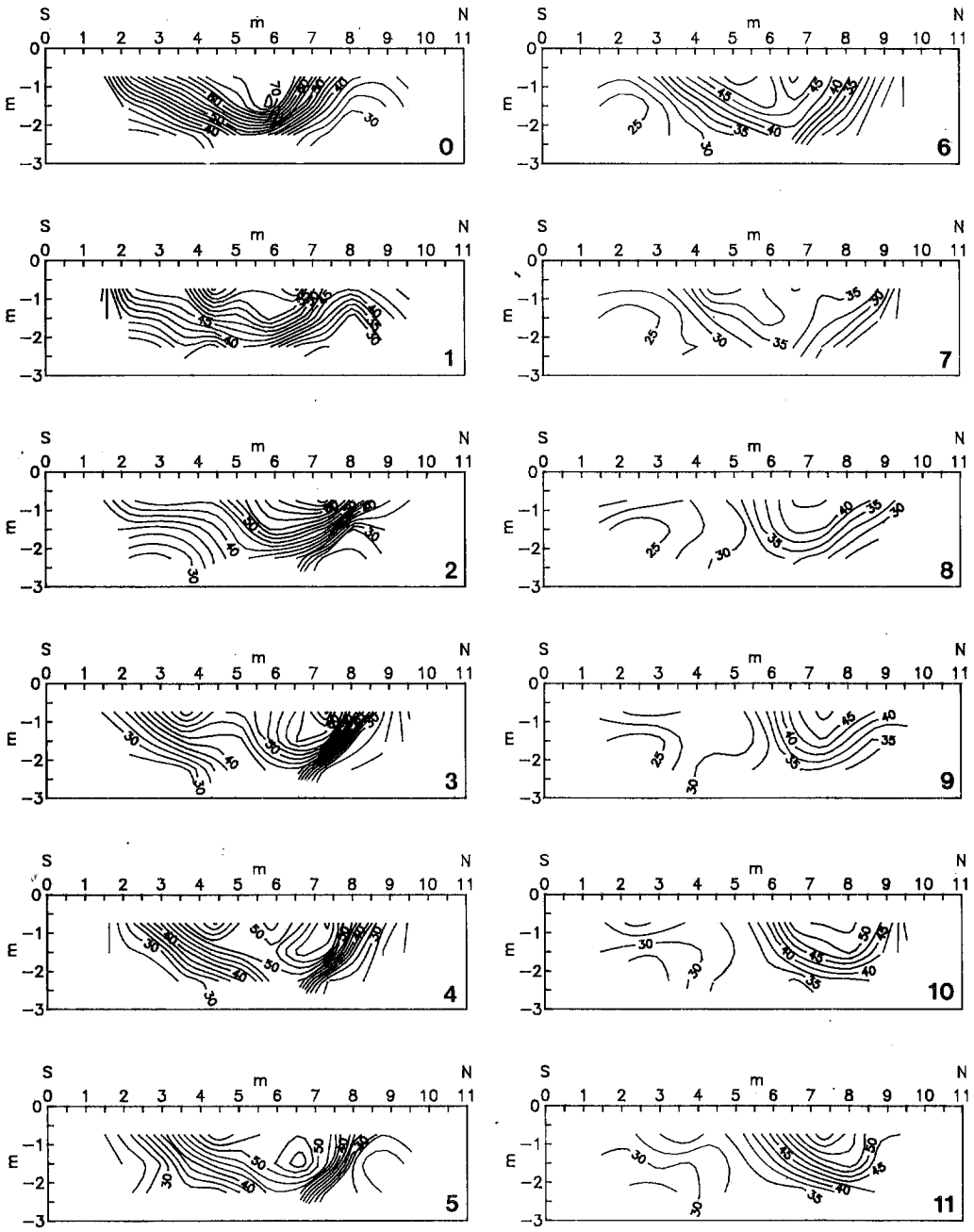

Fig. 15 — Set of pseudo-sections from axial dipole resistivity data (measured in S-N direction) from west (0) to east (11).

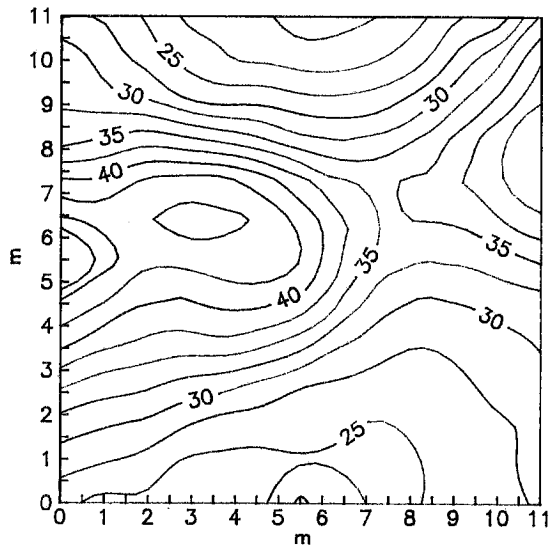

Fig. 16 — Map of all the axial dipole data processed using the Fraser filtering technique along the whole investigated profiles.

yield, with minor uncertainties, $b=1.033$, $c=0.939$, $d=0.909$. So that, as the investigation depth is different for the three arrays (Edwards, 1977), these results would suggest that no very large variations in resistivity are present vertically, at least insofar as the shallow layers are concerned.

The residuals of the linear regression analysis given by eqn. (11) seem to be randomly distributed in the resistivity domain, even if a low-pass filtering procedure appears to enhance a particular non-linear trend (Fig. 6). This resistivity-dependence of the b-residuals means that a non-linear regression should have a better fitting, while their space behaviour can be observed in Fig. 7, where a good correlation with the behaviour of the resistivity data is evident. This good correlation implies that the physical heterogeneities are non-randomly distributed: a model could thus be inferred in which a slow variation of a depth-dependent parameter is predominant.

In the spatial domain, there is a good correlation between the low-pass filtered distribution of the residuals (about 50% of the total signal level, Fig. 8) and the distribution of the resistivities (for istance, the arithmetic mean values of the three values measured with the tripotential method, Fig. 9). The cut-off frequency corresponding to a maximization of the cross-correlation between

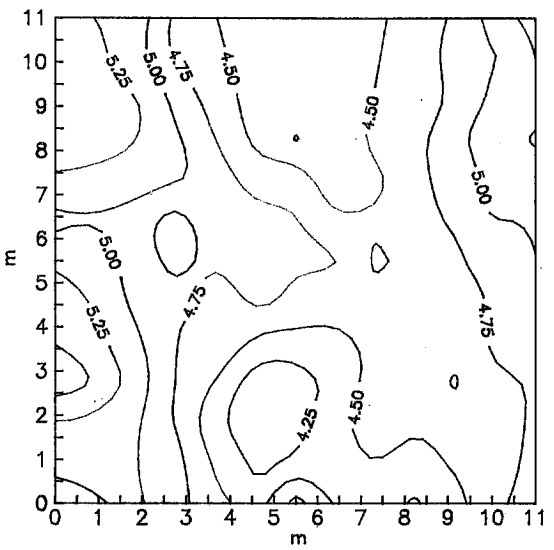

Fig. 17 — Map of the rectangle array. AB=50 m in the W-E direction.

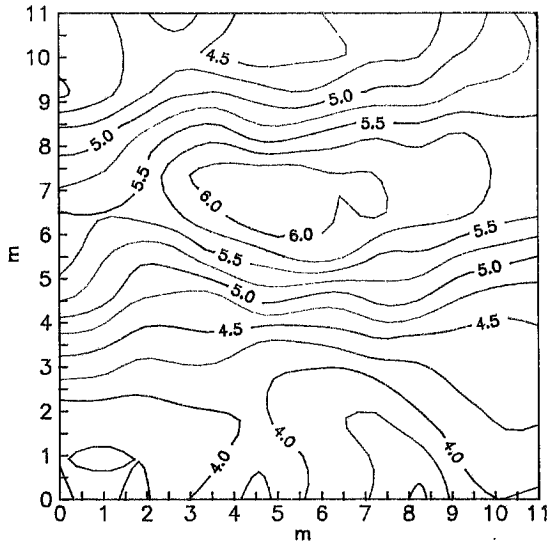

Fig. 18 — Map of the rectangle array. AB=60 m in the N-S direction.

the residuals and the data is useful for designing a spatial low-pass filter to obtain in practice a controlled filtering technique of the data. Some examples of filtered maps are shown in Figs. 10, 11, 12 and 13.

The axial dipole resistivity measurements were used to construct two sets of pseudo-sections (Figs. 14 and 15), respectively in the S-N and W-E directions. In the two sets of sections, it is possible to see a semi-quantitative spatial behaviour of the resistivity isolines, as well as zones characterized by high-gradient variations, both in the vertical and lateral directions. It is also possible to follow the downward prolongations of the superficial traces of the iso-resistivity surfaces shown in the iso-resistivity maps. In particular, a strip with an apparent south-vergent dip angle of 45°, characterized by a high transverse gradient, can be seen to cross the investigated area approximately from ESE to WNW in the north-western part.

A two-dimensional representation of the axial dipole sections was obtained using the Fraser (1981) filtering technique. This map, presented in Fig. 16, can be compared with the resistivity maps previously presented. Even though this map is for a mean investigation depth larger than that of Fig. 13, nevertheless, their general spatial behaviours are very similar: in fact, the low-

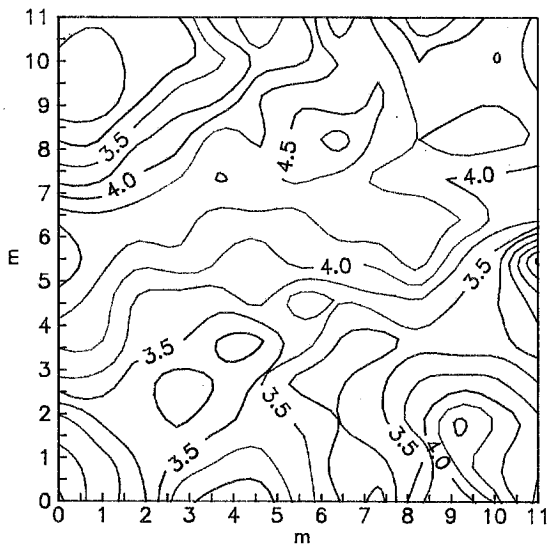

Fig. 19 — Map of the rectangle array. AB=120 m in the N-S directions.

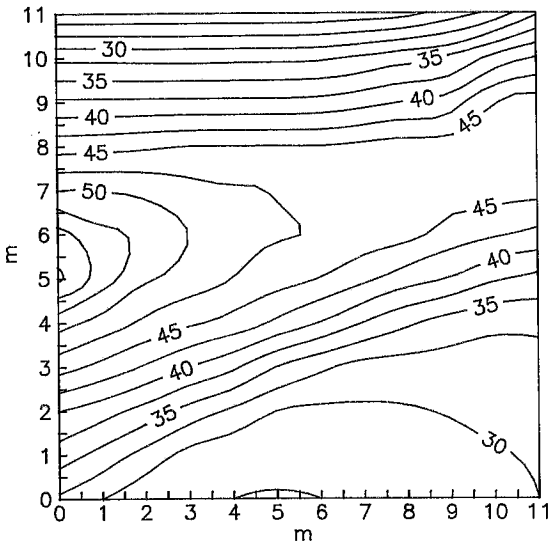

Fig. 20 — Map showing the electrical response of a simple (quasi-bidimensional) model.

pass filtering technique is normaly used to infer deeper characteristics.

Finally, the three filtered maps obtained with the rectangle arrays are shown in Figs. 17, 18 and 19, representing respectively, the W-E rectangle using AB=50 m, and the two N-S rectangles using AB=60 m and AB=120 m. It is easy to recognize large differences both in absolute values and in spatial trend, not only between these maps but also with respect to the previous resistivity maps. It should be stressed that, although characterized by high noise, these maps are correlated with different depths, which on the average are considerably deeper than those previously presented. A possible exception is the map reported in Fig. 18.

Some deep anisotropy can be also inferred by comparison of the behaviours shown in Figs. 17 and 18.

CONCLUSIONS

The majority of the maps indicate a general space behaviour like that presented in Fig. 10.

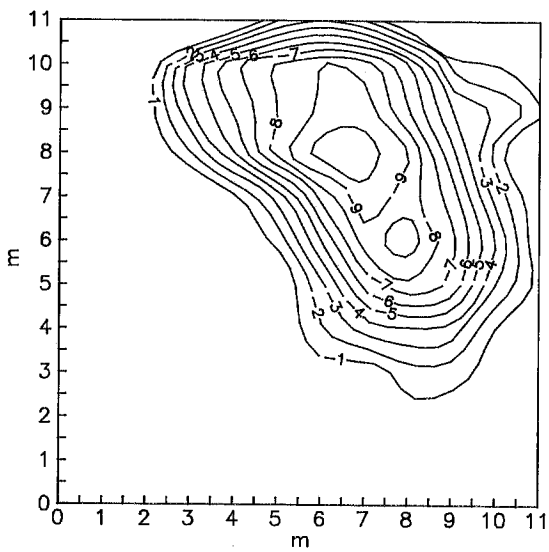

Fig. 21 — Map of the residual anomaly obtained comparing the response of the proposed model and the map of Fig. 10.

Furthermore, the agreement of the shallow and deep investigations suggests that the source of the anomalies is quite large also in the vertical direction: otherwise, it would be characterized by a very high resistivity contrast. To account for this anomaly, both geological or artificial sources are possible.

The spatial behaviour of b (Fig. 7) is very similar to those of the resistivities. So it is probable that the physical source of the behaviour of *b* (typically, resistivity variations in the material located at a depth which is well investigated with one array but not with another) is also responsible for the resistivity spatial behaviours. In particular, a sub-orizontal discontinuity can be hypothesised: its depth should be of the order of the investigated ones and changing according to the trend of the resistivity maps (two layer model: Carpenter and Habberjam, 1956; Cosentino and Luzio, 1992).

Finally, the correspondence between the general trend of the results obtained from this survey and the anomaly recorded using magnetic methods can be recognized by the assumption of a particular "regional" resistivity model. In fact, the simple, nearly two-dimensional regional resistivity model presented in Fig. 20 gives a residual anomaly (Fig. 21) the shape and the position of which are similar to that detected by the magnetic surveys.

Acknowledgements. This paper was also presented a thte "Workshop on geophysical data inversion in archaeological site investigation", held in Berlin on February 18-23, 1992.

REFERENCES

Amadori M.L. and Versino L.; 1991: *Note introduttive alla geologia del parco archeologico di Selinunte*. In: Risultati preliminari delle indagini svolte nell'area archeologica di Selinunte, C.N.R., ITABC, Roma, pp. 1-16.

Bozzo E. and Merlanti F.; 1991: *Misure magnetometriche e geoelettriche sulla collina orientale di Selinunte*. In: Risultati preliminari delle indagini svolte nell'area archeologica di Selinunte, C.N.R., ITABC, Roma, pp.64-95.

Cosentino P. and Luzio D.; 1992: *Trattamento dei dati di misure tripotenziali per Sondaggi Elettrici Orizzontali*. In: Atti del 4° Workshop Nazionale di Geo-Elettro-Magnetismo, Capri 16-18 settembre 1992, in stampa.

Carpenter E.W. and Habberjam G.M.; 1956: *A tri-potential method of resistivity prospecting*. Geophysics, **21**, 455-469.

Edwards L.S.; 1977: *A modified pseudosection for resistivity and induced-polarization*. Geophysics, **42**, 1020-1036.

Fraser D.C.; 1981: *Contour map presentation of dipole-dipole induced polarization data*. Geophysical Prospecting, **29**, 639-651.

Habberjam G.M.; 1979: *Apparent resistivity observations and the use of square array techniques*. Gerbruder Borntraeger, Berlin, 152 pp.

Lapenna V., Mastrantuono M., Patella D. and Di Bello G.; 1991: *Prospezione magnetometrica e geoelettrica nell'area archeologica di Selinunte*. In: Risultati preliminari delle indagini svolte nell'area archeologica di Selinunte, C.N.R., ITABC, Roma, pp. 109-128.

Piro S., Versino L., Feroci M., Brizzolari E., Cardarelli E., Orlando L. and Malagodi S.; 1991: *Applicazione del metodo magnetico, elettromagnetico induttivo ed impulsivo (Georadar) nell'area archeologica di Selinunte - risultati preliminari*. In: Risultati preliminari delle indagini svolte nell'area archeologica di Selinunte, C.N.R., ITABC, Roma, pp. 37-63.